MoO_3 Additives for PVC: A Study of the Molecular Interactions

RICHARD M. LUM, *Bell Laboratories, Murray Hill, New Jersey 07974*

Synopsis

The detailed molecular interactions occurring during thermal degradation of PVC polymer formulations containing MoO_3 additives are investigated using laser microprobe techniques coupled with mass analysis of the volatile pyrolysis products. Comparison with Sb_2O_3–PVC compounds indicate that the additive effects exhibited by MoO_3 are fundamentally different from those observed for Sb_2O_3. Thermal decomposition of MoO_3–PVC is characterized by (1) catalyzed dehydrochlorination of PVC at a lower temperature and increased rate; (2) marked reduction in evolution of benzene, the major fuel species from PVC; and (3) decreased evolution of volatile hydrocarbon species from the polymer plasticizer component. Vapor-phase interactions involving volatile molybdenum species are found to be unimportant. The experimental data indicate that condensed-phase mechanisms and heterogeneous reactions involving $MoO_3(s)$ control polymer decomposition processes. Molecular level details of these reactions are presented and their implications to polymer flame retardance and smoke suppression discussed.

INTRODUCTION

Addition of small amounts of molybdenum trioxide, MoO_3, to polymer formulations has recently been discovered to significantly reduce the amount of smoke generated during combustion. Initial tests[1,2] with plasticized poly(vinyl chloride) (PVC) compounds used in wire and cable materials have indicated reductions in smoke levels of as much as 60%. Little or no loss in flammability rating, as determined by the limiting oxygen index (*LOI*), was observed upon substitution of MoO_3 for antimony trioxide (Sb_2O_3), the standard PVC flame retardant additive. However, full-scale horizontal tunnel (25 ft length) fire tests[3] of cables insulated with various experimental PVC compounds[4] have indicated that the flame spread performance of MoO_3–PVC cables are markedly inferior to Sb_2O_3-containing cables.

A lack of information on the basic chemical and physical interactions governing the MoO_3–PVC system has prevented establishment of any clearly defined mechanism of either MoO_3 smoke suppression or the seemingly contradicting *LOI* and flame spread measurements. In analogy with the Sb_2O_3–PVC interaction,[5–7] the presence of a halogen has been reported[8] as necessary for MoO_3 to be effective—implying the possibility of a gas-phase mechanism. On the other hand, a condensed-phase mechanism is suggested by recent results[9] which indicate that all the molybdenum is accounted for in the contents of the pyrolyzed residue of polymer samples.

In this work the recently developed technique of laser microprobe analysis[7] is used to investigate the MoO_3–PVC interaction. Information on the detailed interactions which occur between the MoO_3 additive and the major vapor species evolved from the PVC substrate is obtained by laser irradiation of MoO_3 isolated in separately controlled atmospheres of HCl and benzene. These data are cor-

Journal of Applied Polymer Science, Vol. 23, 1247–1263 (1979)

0021-8995/79/0023-1247$01.00

related with the results obtained from laser vaporization of PVC samples formulated for wire and cable applications. Measurements are made of the dynamic variations in both the total pressure of the laser-vaporized species in the sample cell and the individual partial pressures of the major volatile components. In addition to the laser microprobe measurements, complementary data are obtained by temperature-programmed pyrolysis coupled with modulated molecular beam mass analysis. Evolution rate curves of the separate pyrolysis fragments are determined from the detailed temperature profiles obtained for the various ion species, and the overall course of the pyrolytic decomposition is directly followed through measurements of the rate of pressure increase in the pyrolysis chamber.

MoO_3 is found to affect the thermal decomposition of PVC in three important respects: (1) MoO_3 acts as a catalyst for the formation of HCl at lower temperatures; (2) evolution of benzene, the major fuel species from PVC, is markedly reduced; (3) evolution of volatile aliphatic species from the polymer plasticizer component is decreased. Evidence is also obtained for the formation of volatile MoO_2Cl_2 species from the reaction between HCl and $MoO_3(s)$. However, the reactivity of MoO_3 is much less than that found for Sb_2O_3. These observations indicate that MoO_3 acts in a much different manner than does Sb_2O_3.

EXPERIMENTAL

PVC samples for both the laser microprobe and temperature-programmed analyses were prepared from the formulations given in Table I. The components were dry blended and milled on a laboratory two-roll mill at 80 psi of steam and then molded into 2-mm-thick specimens. Hydrogen chloride gas and benzene were obtained commercially and used without further purification. Undensified MoO_3 powder was used in the HCl and benzene experiments.

Since details appear elsewhere on the laser microprobe apparatus[7] and temperature-programmed dynamic mass-spectrometric (MS) technique,[10,11] only a brief description is given here. For the MoO_3–HCl and MoO_3–benzene experiments, the MoO_3 powder is isolated in a sample cell (volume ~3 cm^3) directly coupled to the inlet of the MS system via a 0.5-mm-diameter orifice and evacuated through this orifice by the MS vacuum pumps to a background pressure of approximately 10^{-7} torr. After backfilling the cell with from 1 to 100 mtorr HCl or benzene gas, the MoO_3–gas mixture is irradiated with a CO_2 laser beam (λ = 10.6 μm) which enters the cell through a zinc sulfide window. Laser beam

TABLE I
Polymer Compound Formulations

Component	Control, phr[a]	Sb_2O_3–PVC phr	MoO_3–PVC, phr
PVC resin	100	100	100
n-Alkyl phthalate plasticizer	45	45	45
Tribasic lead sulfate	5	5	5
Aluminum oxide trihydrate	50	50	50
Stearic acid	1	0.5	0.5
Petroleum wax	0.5	—	—
Sb_2O_3	—	5	—
MoO_3	—	—	5

[a] phr = Parts per hundred of resin by weight.

intensities are on the order of 10^3 W/cm^2. Reaction products resulting from the MoO_3–gas interaction during laser irradiation are immediately formed into a molecular beam, ionized by electron impact (70 eV electron energy), and analyzed with a quadrupole mass filter. A mechanical chopper operated at a frequency f = 422 Hz is used to modulate the molecular beam. The relative phases of the modulated ion signals are then used to discriminate between molecular ions characteristic of reaction products present in the molecular beam and fragment ions created in the mass spectrometer ion source.[12–14] Simultaneously, the dynamic variations in total pressure in the sample cell during laser irradiation are monitored with an MKS Baratron pressure gauge.

A similar experiment arrangement is used for laser probing of the polymer samples containing the various PVC formulations. Upon laser irradiation, a plume of volatile products is generated from the polymer surface and is sampled using molecular beam techniques. The Baratron pressure gauge enables measurement of the total pressure, which provides information on the overall evolution rate of the thermal decomposition products. The mass filter acts as a partial pressure sensor and, when tuned to a single ionic mass, provides information on the vaporization rate of a given species.

In the temperature-programmed pyrolysis experiments, the polymer samples are heated in a Pyrex glass tube (volume ~60 cm^3) which is attached directly to the inlet of the MS system. Heating rates of 3–10°C/min are employed. As the temperature of the sample tube is increased, gases evolved from the degrading polymer are dynamically sampled via a 0.5-mm-diameter orifice using molecular beam techniques similar to those described above. Throughout the entire pyrolysis run the mass spectrum is automatically scanned in a repetitive mode. Time- and temperature-resolved partial pressure profiles of the pyrolysis product ion signals as well as the variations in total system pressure are thus obtained.

RESULTS AND DISCUSSION

MoO_3–HCl Laser Pyrolysis

Evaluation of a number of metal oxides, especially Group VA metals, has indicated that their effectiveness as flame retardants generally increases when used in combination with a halogen source.[15] It has been established[5–7] that the metal oxide–halogen "synergism" for Sb_2O_3 involves reaction with the halogen source and production of volatile trihalide species. Similar mechanisms have been observed for stannic oxide hydrate[16] ($SnO_2 \cdot H_2O$) and arsenic trioxide[17] (As_2O_3).

To determine whether such a reaction pathway exists for MoO_3, approximately 10 mg powdered MoO_3 was placed in the sample cell and exposed to an atmosphere consisting solely of HCl gas. The composition of the sample cell atmosphere was continuously monitored by mass-spectrometric sampling of the gases effusing through the 0.5-mm cell orifice. A dynamic equilibrium pressure p(cell) = 55 mtorr was maintained. Prior to laser irradiation, only HCl was detected in the gases forming the molecular beam. Unlike the case for Sb_2O_3,[7] no room-temperature reaction leading to the formation of volatile metal halide species was observed for MoO_3.

Upon laser irradiation, however, a sharp decrease was observed in the sample cell pressure with the concomitant appearance of an increasing Mo signal. Total

pressure and Mo partial pressure variations are shown in Figure 1. The mass filter was tuned to the $^{98}Mo^+$ ion signal since this is the most abundant (23.78%) of the seven Mo isotopic species. As the HCl reaction with MoO_3 proceeds, the cell pressure gradually returns to its original value.

The resulting composition of the cell gases was determined by scanning the mass spectrum. As depicted in Figure 2, seven peak clusters were observed, each exhibiting characteristics of the Mo isotopic distribution. Aside from these, the only other peaks observed were due to HCl. Although the spectrum appears complex, the isotopic patterns formed by the various combinations of the seven Mo and two Cl isotopes serve as definite identifying "fingerprints" of the ionic species present. This is illustrated in Table II which presents a comparison of the calculated relative intensities of the assigned species in the third peak cluster (m/e = 124–137) with observed values. Comparison of calculated and observed values for the other peak clusters detected in Figure 2 yields similar results.

However, more than the signal amplitude information is required to determine

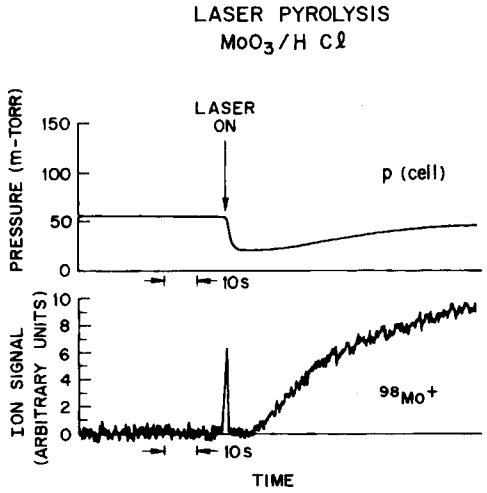

Fig. 1. Dynamic variations observed in cell total pressure and molybdenum partial pressure ($^{98}Mo^+$ isotopic mass signal) during laser pyrolysis of $MoO_3(s)$ isolated in an $HCl(g)$ atmosphere.

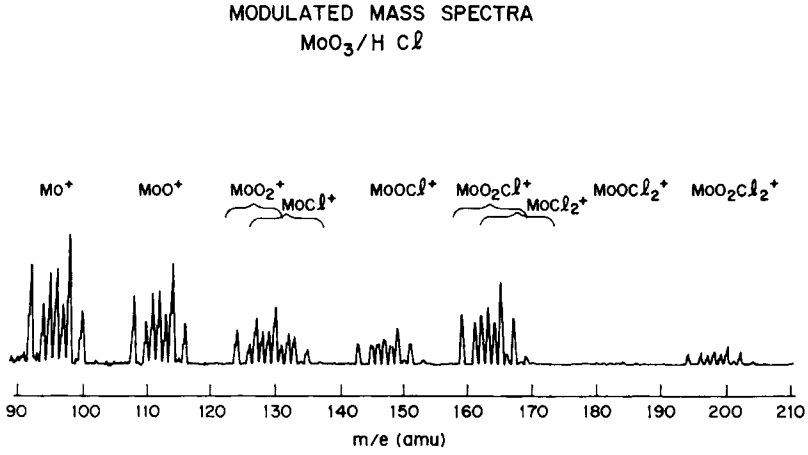

Fig. 2. Ion spectrum characteristic of volatile molybdenum species generated upon laser irradiation of $MoO_3(s)$–$HCl(g)$ system.

TABLE II
Relative Isotopic Abundances

m/e	Species	I(calc)	I(obs)
124	$^{92}MoO_2^+$	0.51	0.58
126	$^{94}MoO_2^+$	0.29	0.35
127	$^{95}MoO_2^+$ / $^{92}Mo^{35}Cl^+$	0.74	0.80
128	$^{96}MoO_2^+$	0.53	0.57
129	$^{97}MoO_2^+$ / $^{94}Mo^{35}Cl^+$ / $^{92}Mo^{37}Cl^+$	0.52	0.59
130	$^{98}MoO_2^+$ / $^{95}Mo^{35}Cl^+$	1.00	1.00
131	$^{96}Mo^{35}Cl^+$ / $^{94}Mo^{37}Cl^+$	0.30	0.32
132	$^{100}MoO_2^+$ / $^{97}Mo^{35}Cl^+$ / $^{95}Mo^{37}Cl^+$	0.52	0.53
133	$^{98}Mo^{35}Cl^+$ / $^{96}Mo^{37}Cl^+$	0.44	0.47
134	$^{97}Mo^{37}Cl^+$	0.04	0.04
135	$^{100}Mo^{35}Cl^+$ / $^{98}Mo^{37}Cl^+$	0.26	0.25
137	$^{100}Mo^{37}Cl^+$	0.04	0.04

whether the ions detected (e.g., MoO_2^+, $MoCl^+$, $MoOCl^+$) are characteristic of reaction product species present in the sample cell or, instead, merely ionization fragments created during electron bombardment of a higher molecular weight parent molecule. Sorting such fragment ions from molecular ions is accomplished by utilizing the phase information contained in the modulated ion signals.

Phase Spectrometry—Identification of Volatile Mo Species

Measured phase values of the modulated ion signals depend upon the molecular and ionic transit times of a given species in the molecular beam. Heavier molecules have longer transit times and therefore correspondingly larger phase lags than those associated with lighter molecules. Detailed discussions of the exact relationships are presented in references 12 to 14. In general, a fragment ion will possess a larger phase lag than a molecular ion corresponding to the same mass-to-charge ratio since the fragment ion is actually associated with a higher molecular weight species and, thus, a longer molecular transit time.

These relationships are illustrated in Figure 3, where the measured ion signal phases resulting from a modulated beam containing an air–benzene mixture are plotted. Phases of the known molecular ions (H_2O^+, N_2^+, O_2^+, Ar^+, and $C_6H_6^+$) fall along the solid line in the figure. However, although separated by only 1 amu, the m/e = 39 fragment ion signal from benzene ($C_3H_3^+$) has a measured phase approximately 20° larger than that associated with the m/e = 40 molecular ion signal from argon. The dashed line represents the predicted phase values for fragment ions from a particular parent (e.g., C_6H_6 and N_2). That is, in addition

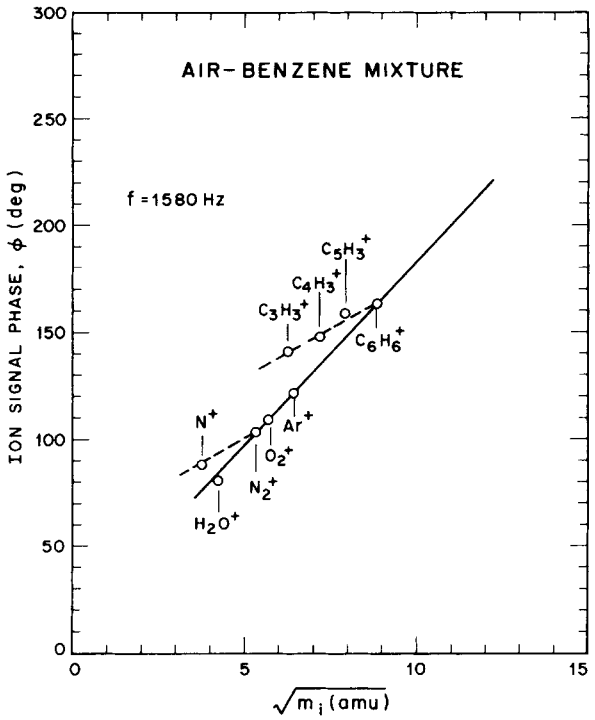

Fig. 3. Phase measurements of modulated ion signals detected from air–benzene mixture: solid line characteristic of molecular ions; dashed line characteristic of fragment ion spectrum from benzene and molecular nitrogen.

to discriminating between fragment and molecular ions, it is also possible, for uncomplicated spectra, to identify the neutral precursor species responsible for a given fragment ion. In this way, known gas mixtures are used to essentially "calibrate" the phase scale for molecular and fragment ions.

Phase measurements for the modulated ion signals resulting from the HCl–MoO_3 interaction are presented in Figure 4. Clearly, only the HCl^+ and $MoO_2Cl_2^+$ signals represent molecular ions. The remaining Mo ionic species in the spectrum of Figure 2 result from fragmentation of molybdenum dioxydichloride (MoO_2Cl_2). Volatile oxide and trihalide species are not observed.

An indication of the relative reactivity of MoO_3 and Sb_2O_3 with HCl can be obtained from the phase measurements characteristic of the two metal oxides. Shown in Figure 5 are the modulated ion signal phases associated with the ionic species resulting from the Sb_2O_3–HCl reaction. Here, a phase difference of approximately 20° is observed between the $^{35}Cl^+$ and $H^{35}Cl^+$ ions, and similarly between $^{37}Cl^+$ and $H^{37}Cl^+$, compared to the essentially equal values observed in Figure 4 for these ions. Obviously, in the Sb_2O_3 system, HCl is not the parent molecule of the Cl^+ ion, but rather $SbCl_3$. Thus, the contribution to the Cl^+ signal due to dissociative ionization of $SbCl_3$ completely dominates that arising from fragmentation of HCl, indicating that a much more extensive reaction occurs between HCl and Sb_2O_3 than with MoO_3.

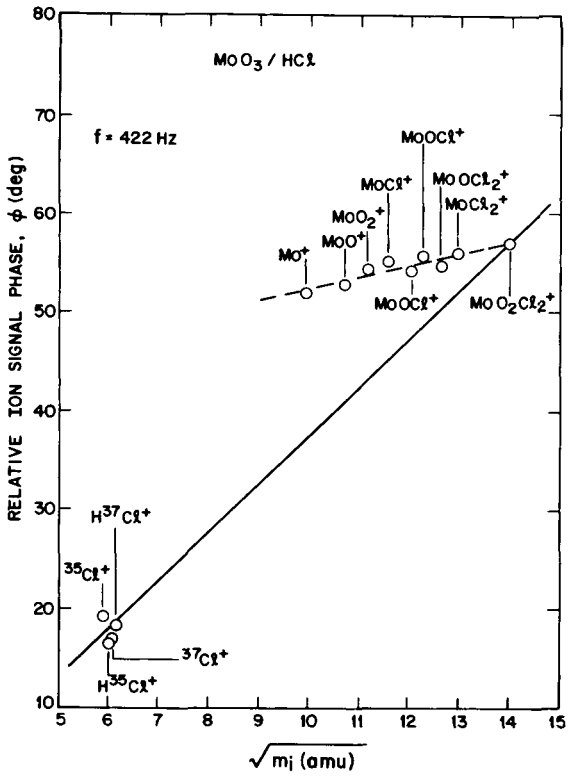

Fig. 4. Phase measurements of modulated ion signals detected during laser pyrolysis of $MoO_3(s)$–$HCl(g)$. The only molecular ions detected are HCl^+ and $MoO_2Cl_2^+$. All other ions are fragments produced upon electron bombardment of these two species.

Laser Microprobe Analysis of PVC Compounds

The influence of MoO_3 on the decomposition process of PVC was examined through its effects on the composition and relative vaporization rates of the volatile species released from the polymer substrate. Laser pyrolysis of flexible PVC samples containing the different formulations specified in Table I was performed for comparative purposes. In addition, a laser target sample consisting of pure unplasticized PVC, obtained by compression molding of the resin powder at 180°C, was used as a control.

Contrary to the MoO_3–HCl experiment, no trace of MoO_2Cl_2 species was observed in high mass scans (m/e = 90–200 amu) of the laser-vaporized products from the PVC formulation containing 5 phr MoO_3. None of the characteristic Mo isotopic peak clusters observed in Figure 2 was detected. However, easily detectable $SbCl_3$ signals were observed upon laser vaporization of the PVC sample containing 5 phr Sb_2O_3, as shown in Figure 6, providing confirming data on the higher reactivity of Sb_2O_3 with HCl.

Evidence of the effects of the MoO_3 additive on the decomposition products from PVC is contained, however, in the low mass (m/e = 12–100 amu) spectral scans presented in Figure 7. These spectra were obtained from separate laser-

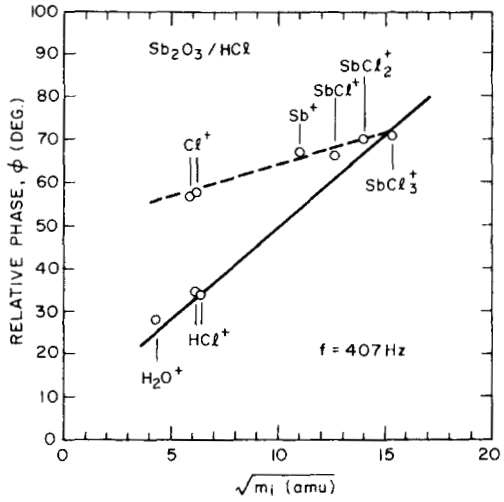

Fig. 5. Phase measurements of modulated ion signals detected from $Sb_2O_3(s)$–$HCl(g)$ system. The Cl^+ signals are produced mainly by dissociative ionization of $SbCl_3$ rather than fragmentation of HCl (compare with Fig. 4).

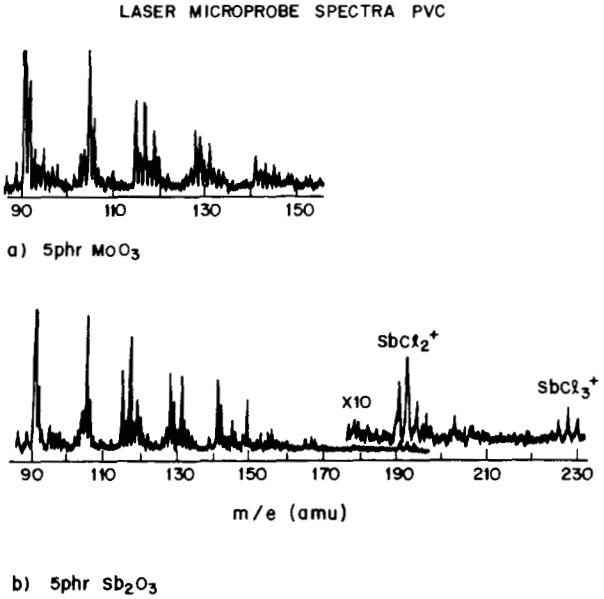

Fig. 6. Ion spectra (m/e = 90–230 amu) characteristic of the laser-vaporized products from: (a) PVC with 5 phr MoO_3; (b) PVC with 5 phr Sb_2O_3.

probe experiments with the four different samples. Although sample geometries were similar, differences in absorption characteristics affect the detailed evolution rate profiles[18] of the volatile species from the four samples. Thus, relative concentrations of pyrolysis products cannot be directly compared from one spectrum to another. However, several qualitative differences in these spectra are evident.

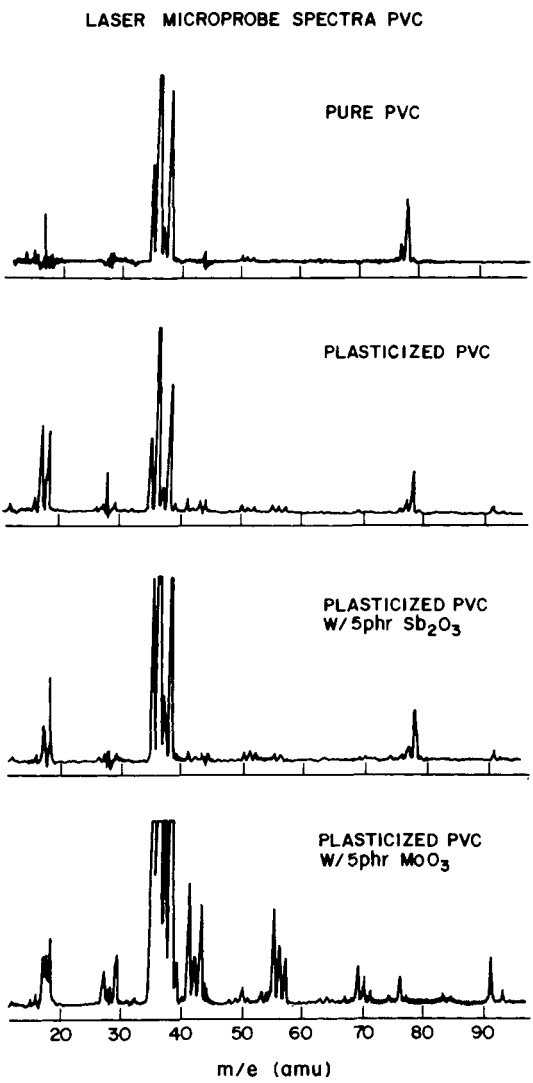

Fig. 7. Ion spectra (m/e = 10–100 amu) characteristic of the laser-vaporized products from pure PVC resin and polymer formulations containing plasticizer and additive components.

Laser vaporization of unplasticized PVC containing no additives yields HCl and benzene as the major volatile products. This is shown in the top spectrum of Figure 7. Addition of plasticizing agents to PVC leads to significant evolution of toluene, as indicated in the second spectrum of Figure 7. Formation of a number of lower molecular weight hydrocarbons also occurs during pyrolysis of the plasticizer, as evidenced by the appearance of peaks at m/e = 39–60. However, HCl and benzene continue to be the major species evolved. A similar low-mass spectrum is observed for the Sb_2O_3–PVC formulation, indicating that the $SbCl_3$ produced by the Sb_2O_3–HCl reaction does not enter into secondary reactions with other volatile species during the thermal decomposition process. The last spectrum of Figure 7 characterizes the products observed during laser pyrolysis of the MoO_3–PVC sample. Again, elimination of HCl from the polymer backbone dominates the volatile products with smaller peaks present due to

decomposition of the plasticizer. However, evolution of benzene, the main organic species observed in the three previous PVC spectra, is virtually eliminated. A more detailed study of these effects, based on data obtained from controlled pyrolysis experiments, is presented in the next section.

The laser microprobe data thus indicate that vapor phase transport of the Mo to the polymer flame zone in the form of volatile MoO_2Cl_2 is unimportant in the mechanism responsible for smoke suppression. Rather, the controlling factor appears to be the striking reduction caused by Mo in the amount of benzene formed in the combustible gases evolved from PVC during thermal degradation. Elimination of benzene as the major fuel species from PVC results in the presence of cleaner burning fuel mixtures composed of aliphatic compounds evolved from the plasticizer component. The extent of carbon formation upon combustion is considerably lower with aliphatic fuels than with aromatic compounds.[19–21]

Temperature-Programmed Pyrolysis of PVC

Total Pressure Measurements

A more detailed study of the effects of the MoO_3 additive on PVC decomposition was performed through controlled pyrolysis at 4°C/min of PVC samples containing plasticizer only (control), 5 phr Sb_2O_3, and 5 phr MoO_3. Measurements were obtained on the overall thermal degradation rate by monitoring the pressure increase corresponding to polymer weight loss through volatilization during pyrolysis.

The resulting pressure profiles for the three PVC samples are presented in Figure 8. Although onset of volatilization is observed at approximately the same temperature for each sample, the initial pressure increase is much more abrupt for the MoO_3–PVC system. The maximum degradation rate for MoO_3–PVC occurs at a temperature 50°–60°C lower than that observed for either the control or Sb_2O_3–PVC. Thermal decomposition of the latter two samples is characterized by a more gradual multi-stage vaporization process. The total pressure data are confirmed by recent thermogravimetric measurements[22] which indicate that the major sample weight loss, in both nitrogen and air atmospheres, occurs at lower temperatures for the MoO_3–PVC samples.

HCl Evolution

Evolution rate curves of the major species generated during degradation of the polymer samples in Figure 8 were determined from the simultaneous ion current measurements made with the mass analyzer. Mass chromatograms of selected ion species representing HCl (m/e = 36), benzene (m/e = 78), toluene (m/e = 91), and C_3 to C_6 aliphatic compounds (m/e = 41) are presented in Figure 9.

The catalytic action of MoO_3 on dehydrochlorination at a lower temperature and increased rate is clearly demonstrated in the ion profile plots. Similar accelerated halogen release has been observed[23–26] with other metal oxides (e.g., Fe_2O_3, ZnO, CaO). It has been proposed[26] that the metal oxide acts as an initiator for PVC degradation. Both the metal atom and, to a lesser extent, the oxygen in the oxide, operating via separate mechanisms, participate in the catalytic effect. In the first case an ionic mechanism has been suggested[27,28] in

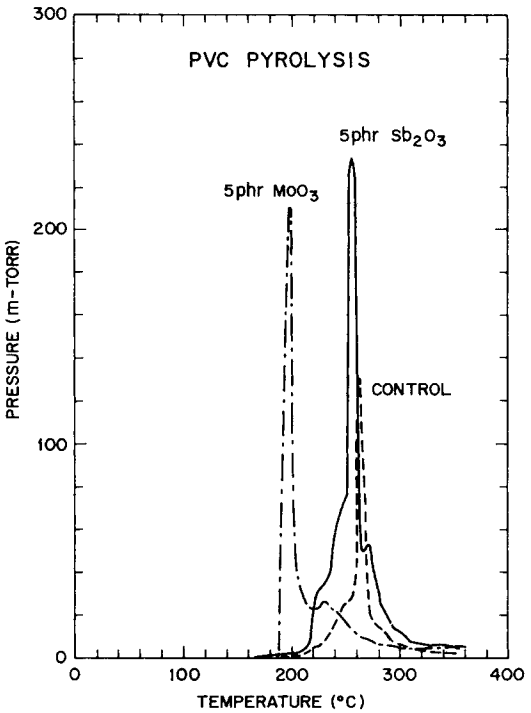

Fig. 8. Dynamic variations observed in cell total pressure during temperature-programmed (4°C/min) pyrolysis of PVC polymer formulations containing plasticizer and additive components.

which the metal atom in the oxide attacks an electronegative chlorine atom in PVC resulting in its abstraction as a chloride anion. This is illustrated by the following reactions which are based on the scheme outlined for Fe_2O_3[26]:

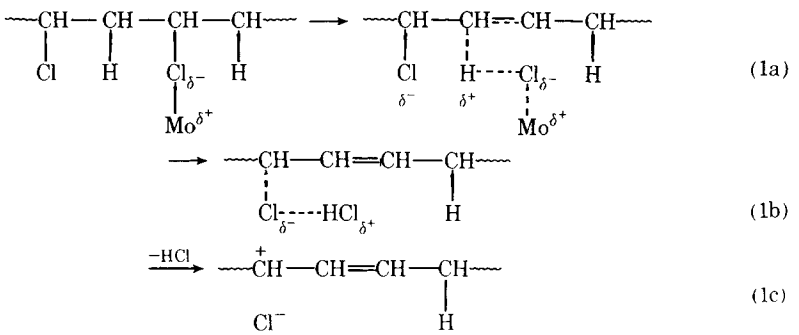

After this initiation stage, further elimination of HCl molecules proceeds in zipper-like fashion by the usual ionic mechanism.[29,30]

Accelerated evolution of HCl during degradation of PVC in the presence of oxygen is well established[29] and is attributed to a radical chain mechanism. The radicals are generated upon polymer chain scission induced by oxygen attack. A similar role is proposed[26] for the behavior of the oxygen in the metal oxide.

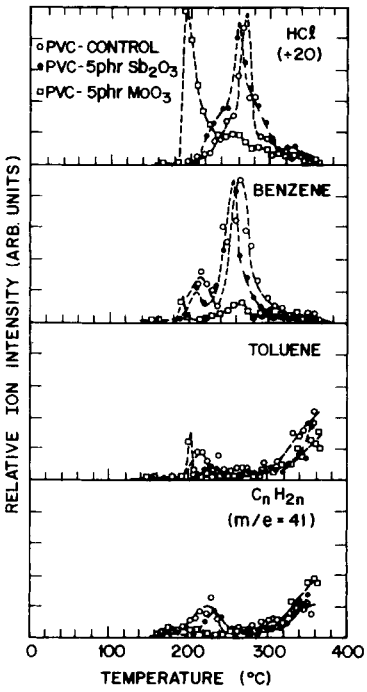

Fig. 9. Product evolution rates determined from mass chromatograms of selected ion species: m/e = 36 (HCl); m/e = 78 (benzene); m/e = 91 (toluene); m/e = 41 (C_3 to C_6 hydrocarbons): (○) PVC–control; (●) PVC–5 phr Sb_2O_3; (□) PVC–5 phr MoO_3.

Benzene, Toluene, and C_nH_{2n} Hydrocarbon Evolution

The specific ion profiles of Figure 9 indicate that for the control and Sb_2O_3–PVC samples, benzene formation occurs in two distinct temperature regimes. Maximum evolution for the first stage coincides with the low-temperature peaks observed for both toluene and C_nH_{2n} species and is therefore attributed to aromatic fragments released during decomposition of the phthalate plasticizer.[31] The more intense second benzene peak occurs simultaneously with the maximum observed in HCl evolution and in this case arises through cyclization of triene units from polyene sequences which form in the degraded polymer as a result of dehydrochlorination[32–34]:

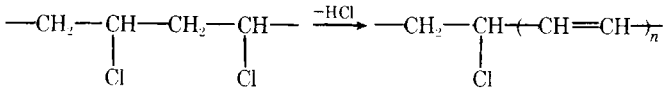

(2)

Mo inhibition of benzene evolution from PVC is clearly evident from the ion profiles of Figure 9, which confirm the laser microprobe observations. The extent of benzene suppression by MoO_3 is indicated in Figure 10, where the benzene: toluene signal ratio is plotted as a function of temperature. Initial formation of benzene, coincident with HCl evolution at T = 190°C, is rapidly quenched. A secondary peak in benzene evolution is observed as the temperature is increased to 260°C. At this temperature HCl evolution from the MoO_3–PVC

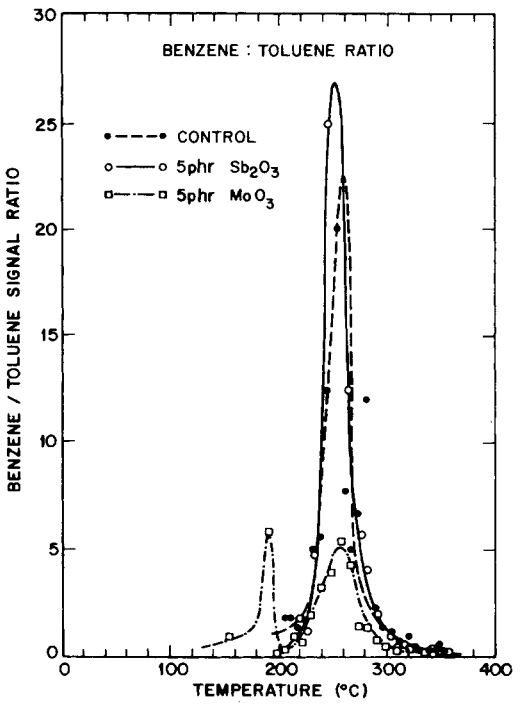

Fig. 10. Mo inhibition of benzene evolution demonstrated by variations observed in the benzene:toluene signal ratio characteristic of PVC polymer formulations containing plasticizer and additive components: (● - - ●) control; (○ — ○) 5 phr Sb_2O_3; (□ — · — □) 5 phr MoO_3.

sample is still significant, as illustrated in Figure 9, and formation of benzene may occur due to decreased efficiency in Mo inhibition at high temperatures. A more detailed discussion of the MoO_3–C_6H_6 interaction will be given in the next section.

In addition to inhibition of benzene, MoO_3 also decreases the low-temperature evolution of toluene and lower molecular weight hydrocarbons characterized by the m/e = 41 ion fragment. Production of volatile "fuel" species from the polymer compound is thus markedly reduced. A similar effect on plasticizer decomposition has been reported[24] for Fe_2O_3.

MoO_3–Benzene Laser Pyrolysis

Suppression of benzene evolution from PVC may occur through (1) direct attack of the formation mechanism, i.e., prevention of the growth of conjugated double bonds along the polymer chain, or (2) immediate uptake of benzene upon formation via heterogeneous reactions. The initial evolution "spikes" observed in the ion profiles of Figure 9 for benzene and toluene suggest gas–solid reactions as the controlling factor. To investigate this possibility powdered MoO_3 was isolated in an atmosphere of benzene vapor kept at a pressure p(cell) = 1.0 mtorr. In a manner similar to the laser pyrolysis of MoO_3–HCl, the composition of the sample cell atmosphere was monitored by mass-spectrometric sampling of the gases effusing through the 0.5-mm cell orifice. Simultaneous measurements were made of the dynamic variations in cell total pressure and benzene partial pressure just before and immediately after laser irradiation of the mixture.

Although the only volatile species detected in either case was benzene, the total and partial pressure measurements presented in Figure 11 provide clear evidence for the occurrence of heterogeneous interactions. Upon laser irradiation, a simultaneous increase by approximately a factor of 2 is observed in both the total pressure and the benzene ion signal. This increase in benzene signal is attributed to laser-stimulated desorption of adsorbed or chemisorbed benzene species from $MoO_3(s)$. These results may be interpreted in terms of π-bonded adsorbed states in which the benzene ring is bound parallel to the surface, e.g., by formation of relatively stable π-bonded complexes as shown below:

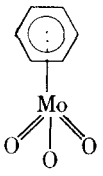

(3)

It is considered[35] that the π-adsorbed state will have a binding energy intermediate between that of van der Waals' adsorption and of dissociative chemisorption via a carbon–metal σ-bond. Similarly, formation of π-olefin complexes[36] could account for the reduced evolution of alkenes observed in Figure 9.

Molybdenum possesses a rich organometallic chemistry,[37] and bridged complexes have been observed[38] for molybdenum oxides of various oxidation states

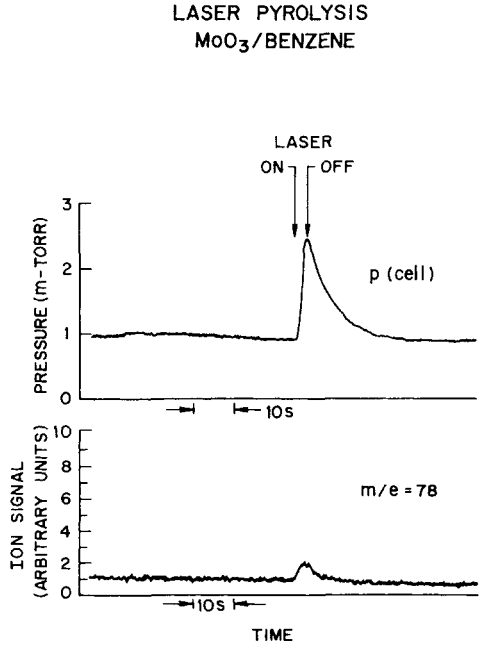

Fig. 11. Dynamic variations observed in cell total pressure and benzene (m/e = 78) partial pressure during laser pyrolysis of $MoO_3(s)$ isolated in a benzene vapor atmosphere.

with cyclopentadienyl as illustrated below:

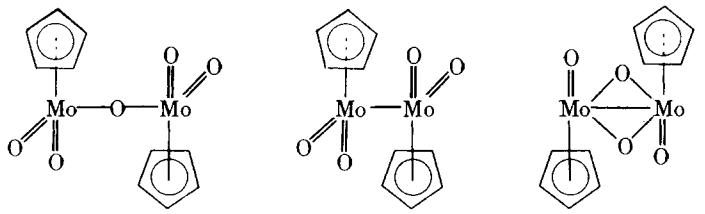

(4)

In addition, a number of bis(arene) "sandwich" compounds have been synthesized[39] using atomic Mo with benzene and toluene ligands:

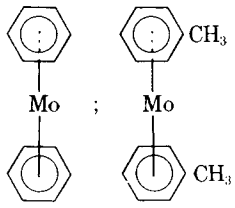

(5)

Formation of elemental Mo through reduction of MoO_3, however, occurs at elevated temperatures ($T > 450°C$) which may exceed the thermal stability of the π-arene complexes shown above.

Although π-bonding may not be an important mechanism at such temperatures, carbon reduction of MoO_3 may partially account for improvements noted in smoke suppression for MoO_3–PVC systems. In experiments with pressed carbon–MoO_3 specimens heated in quartz vessels, a rapid reaction of C with MoO_3 was observed[40] which resulted in the removal of carbon from the reaction zone as gaseous oxides:

$$MoO_3 + 3C \rightarrow Mo + 3CO \quad (6)$$

$$2MoO_3 + 3C \rightarrow Mo + 3CO_2 \quad (7)$$

Also, molybdenum was observed[41] as the reduction product in arc-vaporization studies of MoO_3 mixtures with various organic compounds. However, arc temperatures were on the order of 4000°C, and sample (anode) temperatures were estimated to be about 1000°C. More detailed and controlled thermochemical studies are required for further clarification of the MoO_3 chemistry.

CONCLUSIONS

The detailed mechanisms responsible for the additive effects exhibited in MoO_3–PVC compounds are fundamentally different from those observed for Sb_2O_3–PVC. Vapor-phase transport of Mo to the polymer flame zone is unimportant. Heterogeneous reactions between the metal oxide and the major volatile species evolved from the polymer govern the molecular level interactions of MoO_3 with PVC instead. The catalyzed dehydrochlorination of PVC at a lower temperature and increased rate is initiated by an ionic mechanism involving the molybdenum atom of the oxide, with the oxygen in the oxide perhaps participating to a lesser degree via a radical mechanism that induces chain scission. Evolution of benzene and toluene from the polymer is inhibited by a chemi-

sorption process apparently involving the formation of relatively stable π-arene complexes with MoO_3. A similar π-bonding mechanism involving Mo-olefin complexes is suggested by the decreased evolution observed in C_3 to C_6 hydrocarbons from the plasticizer component of the polymer.

The flame retardant properties of MoO_3 as reflected in the *LOI* measurements can thus be attributed to the early release of HCl which acts as a radical scavenger in the flame front. Conversely, reduced concentrations of relatively "dirty" aromatic fuel species in the combustible gases evolved from the polymer, especially benzene, account for the decreased smoke levels observed for MoO_3–PVC compounds. Although these additive effects result in favorable flammability ratings for the compound by several tests, overall they have a destabilizing effect on the polymer since degradation is initiated at a lower temperature and a relatively flammable char residue is produced. This is confirmed by the observed failure of the MoO_3 additive to arrest flame spread in the horizontal tunnel cable fire tests.

The author is especially grateful to V. J. Kuck for valuable insights gained from discussions of her experimental results on the flammability and smoke inhibition properties of MoO_3 additives. Further acknowledgments are due to E. Scalco for his helpful comments on PVC–additive interactions in general and to L. Seibles for informative discussions on the organometallic chemistry of MoO_3. All polymer formulations used in this study were kindly provided by E. Scalco.

References

1. D. A. Church and F. W. Moore, *Plast. Eng.*, **31,** 36 (1975).
2. V. J. Kuck, private communication.
3. S. Kaufman and M. M. Yocum, private communication.
4. E. Scalco, private communication.
5. J. J. Pitts, P. H. Scott, and D. G. Powell, *J. Cell. Plast.*, **6,** 35 (1970).
6. J. W. Hastie, *J. Res. Natl. Bur. Stand.*, **77A,** 733 (1973).
7. R. M. Lum, *J. Polym. Sci., Polym. Chem. Ed.*, **15,** 489 (1977).
8. *Plast. Technol.*, "Flame Retardants: R&D Pace Quickens" p. 51, July 1976.
9. F. W. Moore and D. A. Church, paper presented at 1976 International Symposium on Flammability and Fire Retardants, Toronto, Ontario, Canada, May 1976.
10. R. M. Lum, *ACS Polym. Prepr.*, **18,** 761 (1977).
11. R. M. Lum, *J. Polym. Sci., Polym. Chem. Ed.*, **17,** 203 (1979).
12. J. Fricke, W. M. Jackson, and W. L. Fite, *J. Chem. Phys.*, **57,** 580 (1972).
13. W. L. Fite, *Int. J. Mass Spectrom. Ion Phys.*, **16,** 109 (1975).
14. R. M. Lum, *Thermochim. Acta,* **18,** 73 (1977).
15. J. J. Pitts, *J. Fire Flamm.*, **3,** 51 (1972).
16. J. Touval, *J. Fire Flamm.*, **3,** 130 (1972).
17. R. M. Lum, unpublished results.
18. R. M. Lum, *J. Appl. Polym. Sci.*, **20,** 1635 (1976).
19. V. J. Kuck, private communication.
20. K. H. Homann and H. G. Wagner, Proc. 11th International Symposium on Combustion, Berkeley, California 1967, p 371.
21. A. M. Calcraft, R. J. S. Green, and T. S. McRoberts, *Plast. Polym.*, **42,** 200 (1974).
22. V. J. Kuck and E. Scalco, paper presented at 34th Annual Technical Conference of the Society of Plastics Engineers, Atlantic City, New Jersey, April 1976.
23. M. A. Dudley and D. A. Smith, in *Advances in Polymer Science and Technology,* S.C.I. Monograph No. 26, Society of Chemistry Industry, London, 1967, p. 49.
24. P. Dunn and B. C. Ennis, *J. Appl. Polym. Sci.*, **14,** 355 (1970).
25. E. R. Wagner and B. L. Joesten, *J. Appl. Polym. Sci.*, **20,** 2143 (1976).
26. Y. Uegaki and T. Nakagawa, *J. Appl. Polym. Sci.*, **21,** 965 (1977).
27. I. Mochida, J. Take, Y. Saito, Y. Yoweda, and T. Seiyama, *J. Catalysis,* **18,** 33 (1970).
28. I. A. Abu-Isa, *J. Polym. Sci. A-1,* **10,** 881 (1972).
29. W. C. Geddes, *Rubber Chem. Technol.*, **40,** 177 (1967).

30. D. Braun, in *Degradation and Stabilization of Polymers,* G. Geuskens, Ed., Halsted Press, New York 1975, p. 23.

31. J. H. Futrell, D. A. Chatfield, F. D. Hileman, K. J. Voorhees, and I. N. Einhorn, *ACS Polym. Prepr.,* **17,** 767 (1976).

32. E. P. Chang and R. Salovey, *J. Polym. Sci., Polym. Chem. Ed.,* **12,** 2927 (1974).

33. G. A. Rasuvaev, L. S. Troitskaya, and B. B. Troitskii, *J. Polym. Sci., Polym. Chem. Ed.,* **9,** 2673 (1971).

34. R. R. Stromberg, S. Straus, and B. G. Achhammer, *J. Polym. Sci.,* **35,** 355 (1959).

35. J. R. Anderson and B. G. Baker, in *Chemisorption and Reactions on Metallic Films,* Vol. 2, J. R. Anderson, Ed., Academic Press, New York, 1971, p. 154.

36. K. J. Klabunde, *Acc. Chem. Res.,* **8,** 393 (1975).

37. D. J. Darensbourg and M. Y. Darensbourg, *J. Organomet. Chem.,* **115,** 221 (1976).

38. M. Cousins and M. L. H. Green, *J. Chem. Soc.,* 1567 (1964).

39. M. P. Silvon, E. M. Van Dam, and P. S. Shell, *J. Am. Chem. Soc.,* **96,** 1945 (1974).

40. Yu. A. Pavlov, S. N. Kryukov, S. B. Sheboldaev, and G. Ya. Meshcheryakov, *Inorg. Mater.,* **11,** 567 (1975).

41. A. Delÿska, Chr. Prăvčeva, and N. Tončev, *Spectrochim. Acta,* **31B,** 121 (1976).

Received December 9, 1977
Revised February 3, 1978